

*Dedicated*

*To my beloved parents*



## CERTIFICATE

It is certified that the work contained in the thesis titled "**STRUCTURAL, MAGNETIC AND ELECTROCHEMICAL PROPERTIES OF MULTIFUNCTIONAL NANOSTRUCTURED POLYMORPHS OF MnO<sub>2</sub> AND Dy DOPED MnO<sub>2</sub>**" by "**DEEPTI GANGWAR**" has been carried out under my supervision and that this work has not been submitted elsewhere for a degree.

It is further certified that the student has fulfilled all the requirements of Comprehensive, Candidacy and SOTA for the award of Ph.D. degree.

Date: 10th Nov 2021

Place: Varanasi

*Chandana Rath*

Dr. (Mrs. Chandana Rath)  
(Supervisor)

Associate Professor/सह-आचार्य  
School of Materials Science & Technology/पदार्थ विज्ञान एवं प्रौद्योगिकी स्कूल  
Indian Institute of Technology/भारतीय प्रौद्योगिकी संस्थान  
(Banarus Hindu University), Varanasi/कशी हिन्दू विश्वविद्यालय, वाराणसी



## DECLARATION BY THE CANDIDATE

I, **DEEPTI GANGWAR**, certify that the work embodied in this Ph.D. thesis is my own bonafide work carried out by me under the supervision of **Dr. (Mrs.) CHANDANA RATH** for a period from **July 2016** to **Nov 2021** at the **SCHOOL OF MATERIALS SCIENCE AND TECHNOLOGY**, Indian Institute of Technology (Banaras Hindu University), Varanasi, India. The matter embodied in this Ph.D. thesis has not been submitted for the award of any other degree/diploma. I declare that I have faithfully acknowledged and given credits to the research workers wherever their works have been cited in my work in this thesis. I further declare that I have not willfully copied any other's work, paragraphs, text, data, results, *etc.*, reported in journals, books, magazines, reports, dissertations, thesis, *etc.*, or available at websites and have not included them in this thesis and have not cited as my own work.

Date...*10th Nov 2021*.....

Place: Varanasi

*Deepti*  
(DEEPTI GANGWAR)

## CERTIFICATE BY THE SUPERVISOR

This is to certify that the above statement made by the candidate is correct to the best of my knowledge.

*Chandana Rath*  
**Dr. (Mrs.) Chandana Rath**  
**Supervisor**

Associate Professor/सह-आचार्य  
School of Materials Science & Technology/पदार्थ विज्ञान एवं प्रौद्योगिकी स्कूल  
Indian Institute of Technology/भारतीय प्रौद्योगिकी संस्थान  
(Banaras Hindu University), Varanasi/काशी हिन्दू विश्वविद्यालय, वाराणसी

*Chandana Rath*  
**Dr. (Mrs.) Chandana Rath**  
**Coordinator**

Coordinator/समन्वयक  
School of Materials Science & Technology/पदार्थ विज्ञान एवं प्रौद्योगिकी स्कूल  
Indian Institute of Technology/भारतीय प्रौद्योगिकी संस्थान  
(Banaras Hindu University), Varanasi/काशी हिन्दू विश्वविद्यालय, वाराणसी



## **COPYRIGHT TRANSFER CERTIFICATE**

**Title of the Thesis: “*STRUCTURAL, MAGNETIC AND ELECTROCHEMICAL PROPERTIES OF MULTIFUNCTIONAL NANOSTRUCTURED POLYMORPHS OF MnO<sub>2</sub> AND Dy DOPED MnO<sub>2</sub>*”**

**Candidate's Name: Mrs. DEEPTI GANGWAR**

### **Copyright Transfer**

The undersigned hereby assigns to the Indian Institute of Technology (Banaras Hindu University), Varanasi all rights under copyright that may exist in and for the above thesis submitted for the award of the *Doctor of Philosophy*.

Date: 10 Nov. 2021

Place: Varanasi

  
(DEEPTI GANGWAR)

**Note: However, the author may reproduce or authorize others to reproduce materials extracted verbatim from the thesis or derivative of the thesis for author's personal use provided that the source and the Institute's copyright notice is indicated.**



## *Acknowledgements*

*First and Foremost, I wish to express my sincere gratitude to my supervisor **Dr. (Mrs.) CHANDANA RATH**, for giving me an opportunity to join her research group. I am highly obliged and thankful to her for providing me her illustrious guidance, valuable suggestions, encouragement and futuristic vision, which enabled me to develop a better understanding of the subject that lead to the successful completion of the research work. I am indebted to her for cultivating values and confidence in me.*

*I would also like to express my sincere thanks to RPEC member's Prof. Rajiv Prakash, School of Materials Science & Technology, and Dr. Ashutosh Dubey, Department of Ceramic Engineering, Institute of Technology (Banaras Hindu University), for their stimulating help and criticism which incented me to widen my research from various perspectives. I would like to thank coordinator of School of Materials Science and Technology, IIT (BHU) for providing different instrumental facility. I wish to express deep regards to all the faculty members of our school; Prof. D. Pandey, Prof. P. Maiti, Dr. A. K. Singh, Dr. Chandan Upadhyay, Dr. B. N. Pal, Dr. S. K. Mishra, Dr. A. K. Mishra, Dr. Sanjay Singh, Dr. Nikhil Kumar and Dr. S. R. Singh for their encouragement and support.*

*With a deep sense of gratitude, I express my sincere thanks to CIFC, IIT (BHU), Varanasi, for help in carrying characterization of the synthesized samples. I am also grateful to all office staff of the school and authorities of IIT (BHU), for their kind help during the period of my stay to complete the thesis work.*

*I owe my sincerest thanks to my seniors Dr. Himanshu Tripathi, Dr. Priyanka Tiwari, Dr. B. Bharati, Dr. Sandeep Kumar, Dr. Jagadish Kumar G. and Dr. Durgesh Kumar for their valuable advice. It was also a great pleasure to work with my fellow lab mates Mr. Gaurav Chandra Pandey, Mr. Manish Yadav, Mr. Abhay Narayan Singh, Mr. Taranga Dehury, Mr. Akhilesh Yadav and Ms. Sanjana Rajpoot.*

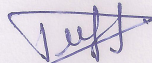
*I am extremely thankful to my friends Dr. Ritu Saxena, Dr. Yamini Khodia Rao, Ms. Mahima Singh, Ms. Vandana Tomar, Ms. Akanksha Yadav and Ms. Monika Singh for their support, cooperation and help in many ways as well as for providing me the homely environment, encouragement during my bad days and making my stay here enjoyable. With special thanks to my husband, Dr. Mohit Kumar, for his unwavering support and understanding, this enabled the thesis to be completed.*

*It fills me with a deep sense of reverence when I think about my family. Their constant encouragement, moral support and cooperation at every step of my life can't be expressed in words. I am thankful for their love and blessings.*

*Finally, I bow with reverence and gratitude to thank the Almighty MAHADEV who has enriched me with such an excellent opportunity and infused the power in my mind to fulfill the work assigned to me.*

Date: 10th Nov. 2021

Place: Varanasi

  
(DEEPTI GANGWAR)

# *Contents*

## ***Contents***

<b><i>Acknowledgements</i></b> .....	<b>ix</b>
<b><i>Contents</i></b> .....	<b>xi</b>
<b><i>List of Figures</i></b> .....	<b>xv</b>
<b><i>PREFACE</i></b> .....	<b>xxvii</b>
<b>Chapter 1 Introduction and Literature Review</b> .....	<b>1</b>
1.1 Introduction.....	1
1.1.1 Crystal Structure .....	2
1.1.2 Magnetic Behaviour.....	6
1.1.3 Applications.....	17
1.2 Literature survey .....	23
1.2.1 Synthesis of the Polymorphs of MnO <sub>2</sub> .....	23
1.2.2 Structural Transformation: Effect of Synthesis Parameters & dopants.....	26
1.2.3 Structure, Morphology and Dopant Dependent Magnetic Properties.....	29
1.2.4 MnO <sub>2</sub> as an Electrode Material for Supercapacitor application .....	31
1.3 Objectives.....	37
<b>Chapter 2 Synthesis and Characterization Techniques</b> .....	<b>41</b>
2.1 Sample preparation.....	41
2.1.1 Hydrothermal Synthesis Technique.....	42
2.2 Characterization Techniques.....	46
2.2.1 X-ray Diffraction (XRD) .....	47
2.2.2 Fourier Transform Infrared Spectroscopy (FT-IR).....	50
2.2.3 Raman spectroscopy .....	51
2.2.4 Scanning Electron Microscope (SEM) .....	53
2.2.5 Transmission Electron Microscope (TEM) .....	54
2.2.6 X-ray Photoelectron Spectroscopy (XPS) .....	56
2.2.7 Brunauer-Emmett-Teller Measurement (BET).....	57
2.2.8 UV-Visible Spectroscopy .....	58
2.2.9 Magnetic Measurements .....	59
2.2.10 Electrochemical Measurements .....	61

<b>Chapter 3 Structure, Optical and Magnetic Properties with electrochemical Performance of <math>\alpha</math> and <math>\beta</math>-MnO<sub>2</sub>Nanorods.....</b>	<b>67</b>
3.1 Introduction .....	67
3.2 Structure, Microstructure and Optical Properties.....	68
3.2.1 Fourier Transform Infrared Spectroscopy .....	68
3.2.2 X-Ray Diffraction: Rietveld Refinement.....	69
3.2.3 Emission Scanning Electron Microscope .....	74
3.2.4 UV Visible Spectroscopy.....	75
3.2.5 X-ray Photoelectron Spectroscopy .....	77
3.3 Electrochemical Performance Using Cyclic Voltammetry .....	80
3.4 Magnetic Properties.....	82
3.4.1 Temperature Dependent Magnetization.....	82
3.4.2 Field Dependent Magnetization.....	84
3.4.3 ac Susceptibility .....	86
3.4.4 Remanent Magnetization Measurement .....	91
3.5 Conclusion.....	94
<b>Chapter 4 Structure, Microstructure and Magnetic Properties of Hydrothermally Synthesized <math>\delta</math>-MnO<sub>2</sub> .....</b>	<b>97</b>
4.1 Introduction .....	97
4.2 Structural and Microstructural Analysis .....	98
4.2.1 X-ray Diffraction .....	98
4.2.2 Fourier Transform Infrared Spectroscopy .....	98
4.2.3 Raman Spectroscopy.....	100
4.2.4 Transmission Electron Microscope.....	101
4.2.5 X-Ray Photoelectron Spectroscopy .....	102
4.3 Magnetic Properties.....	104
4.3.1 Temperature Dependent Magnetization.....	104
4.3.2 Field Dependent Magnetization.....	109
4.3.3 ac Susceptibility .....	110
4.3.4 Remanant Magnetization Measurement .....	115
4.4 Conclusion.....	118
<b>Chapter 5 Electrochemical Studies of Dy Doped <math>\alpha</math>-MnO<sub>2</sub> Nanorods for Supercapacitor Application .....</b>	<b>119</b>

5.1	Introduction .....	119
5.2	Structural and Microstructural Analysis .....	120
5.2.1	X-ray Diffraction .....	120
5.2.2	Raman Spectroscopy.....	122
5.2.3	Scanning Electron Microscope .....	123
5.2.4	Transmission Electron Microscope .....	125
5.3	Surface Area Analysis (BET).....	127
5.4	Electrochemical Analysis.....	129
5.4.1	Cyclic Voltammetry.....	129
5.4.2	Galvanostatic Charge Discharge.....	133
5.4.3	Electrochemical Impedance Spectroscopy .....	136
5.5	Conclusion .....	138
<b>Chapter 6 Magnetic Properties of Dy Doped <math>\alpha</math>-MnO<sub>2</sub> Nanorods.....</b>		<b>139</b>
6.1	Introduction.....	139
6.2	X-ray Photoelectron Spectroscopy.....	140
6.3	Magnetic Properties .....	142
6.3.1	Temperature Dependent Magnetization.....	142
6.3.2	Field Dependent Magnetization.....	145
6.3.3	Remanant Magnetization Measurement .....	149
6.3.4	Training Effect.....	150
6.4	Conclusion .....	156
<b>Chapter 7 Conclusions and Future Work .....</b>		<b>157</b>
<b><i>References.....</i></b>		<b>161</b>
<b><i>List of publications.....</i></b>		<b>181</b>



## *List of Figures*

<b>Figure 1.1:</b> MnO <sub>6</sub> octahedral molecular sieve (OMS) and its sharing pattern. ....	3
<b>Figure 1.2:</b> Arrangement of various MnO <sub>2</sub> framework by forming tunnel (n x m) structures [38].....	5
<b>Figure 1.3:</b> The magnetization process in ferromagnets.....	8
<b>Figure 1.4:</b> Curie-Weiss law for the ferromagnetic material (a) $\chi$ Vs T and (b) $\chi^{-1}$ Vs T above and below T <sub>C</sub> . ....	8
<b>Figure 1.5:</b> Magnetization M versus applied field H for a ferromagnetic material (Hysteresis loop).....	9
<b>Figure 1.6:</b> (a) Outline of magnetic dipoles in antiferromagnetic material aligns in opposite direction, Curie-Weiss law (b) $\chi$ Vs T and (c) $\chi^{-1}$ Vs T above and below T <sub>N</sub> .....	11
<b>Figure 1.7:</b> Arrangement of spins in different types of antiferromagnetism. ....	11
<b>Figure 1.8:</b> Bathel-Slater curve showing the variation of exchange integral with 3d orbital radius r <sub>3d</sub> relative to atomic radius r <sub>a</sub> . ....	14
<b>Figure 1.9:</b> Schematic diagram for (a) superexchange interaction and (b) double exchange interaction. ....	16
<b>Figure 1.10:</b> Various properties of MnO <sub>2</sub> nanostructures.....	19
<b>Figure 1.11:</b> Different applications of MnO <sub>2</sub> nanostructures. ....	20
<b>Figure 1.12:</b> Taxonomy of materials for supercapacitors.....	21
<b>Figure 1.13:</b> Schematic diagram of supercapacitor (a) EDLC and (b) Pseudocapacitor....	21
<b>Figure 1.14:</b> XRD patterns of the different compositions of Zn/Mn mix-MnO <sub>2</sub> .....	28
<b>Figure 1.15:</b> Constrained equilibrium thermodynamics driving phase selection between MnO <sub>2</sub> polymorphs as a function of solution conditions at 298 K and zero applied potential, for solutions containing (a) Li <sup>+</sup> , (b) Na <sup>+</sup> , (c) K <sup>+</sup> , (d) Mg <sup>2+</sup> , or (e) Ca <sup>2+</sup> cations.....	28
<b>Figure 1.16:</b> (a) Galvanostatic charge/discharge curves of MnO <sub>2</sub> and Co-MnO <sub>2</sub> spheres at a current density of 1 A/g (b) cyclic stability of MnO <sub>2</sub> and Co-MnO <sub>2</sub> at a current density of 2 A/g. ....	33
<b>Figure 2.1:</b> Flow chart for the synthesis of MnO <sub>2</sub> using hydrothermal technique. ....	43

<b>Figure 2.2:</b> Flow chart for the Synthesis of $\alpha$ -MnO <sub>2</sub> , $\beta$ -MnO <sub>2</sub> , and $\alpha\beta$ -MnO <sub>2</sub> .....	44
<b>Figure 2.3:</b> Flow chart for the Synthesis of $\delta$ -MnO <sub>2</sub> and $\alpha$ -MnO <sub>2</sub> . .....	45
<b>Figure 2.4:</b> Schematic Flow chart for the synthesis of bare and Dy doped $\alpha$ -MnO <sub>2</sub> .....	46
<b>Figure 2.5:</b> Schematic diagram of incident and diffracted X-rays from the crystal lattice. ....	48
<b>Figure 2.6:</b> Schematic representation of X-ray technique. ....	49
<b>Figure 2.7:</b> Schematic diagram for the simplified setup of Raman spectroscopy. ....	52
<b>Figure 2.8:</b> UV-Visible Spectrophotometer.....	58
<b>Figure 2.9:</b> MPMS-3, Quantum Design (USA) used for magnetic measurement .....	60
<b>Figure 2.10:</b> An electrochemical three electrode setup.....	62
<b>Figure 2.11:</b> Schematic circuit diagram of electrochemical three electrode setup (Potentiostat/Galvanostat, PSTAT/GSTAT).[152].....	63
<b>Figure 3.1:</b> Fourier-Transform Infrared (FT-IR) spectrum of $\alpha$ -MnO <sub>2</sub> , $\beta$ - MnO <sub>2</sub> and $\alpha\beta$ -MnO <sub>2</sub> nanorods. ....	68
<b>Figure 3.2:</b> Room temperature X-Ray diffraction (XRD) pattern of (a) $\alpha$ -MnO <sub>2</sub> , (b) $\gamma$ -MnOOH, and (c) $\alpha\beta$ - MnO <sub>2</sub> nanorods. ....	70
<b>Figure 3.3:</b> X-Ray diffraction (XRD) pattern of $\alpha$ -MnO <sub>2</sub> , $\beta$ -MnO <sub>2</sub> , and $\alpha\beta$ - MnO <sub>2</sub> nanorods calcined at 400° C. ....	71
<b>Figure 3.4:</b> XRD pattern of $\alpha$ -MnO <sub>2</sub> , $\beta$ - MnO <sub>2</sub> and $\alpha\beta$ - MnO <sub>2</sub> nanorods fitted using Rietveld refinement of Fullprof program.....	71
<b>Figure 3.5:</b> Scanning electron micrograph (SEM) of (a) $\alpha$ -MnO <sub>2</sub> , (b) $\beta$ - MnO <sub>2</sub> and (c) $\alpha\beta$ -MnO <sub>2</sub> nanorods. ....	73
<b>Figure 3.6:</b> particle size distribution histogram of (a) $\alpha$ -MnO <sub>2</sub> , (b) $\beta$ - MnO <sub>2</sub> , (c.1) phase 1 and (c.2) phase 2 of $\alpha\beta$ - MnO <sub>2</sub> nanorods. ....	74
<b>Figure 3.7:</b> (a) UV-visible absorption spectra of $\alpha$ -, $\beta$ - and $\alpha\beta$ -MnO <sub>2</sub> nanorods. Tauc plot and the corresponding linear fit for the calculation of optical bandgap of (b) $\alpha$ -MnO <sub>2</sub> , (c) $\beta$ -MnO <sub>2</sub> and (d) $\alpha\beta$ -MnO <sub>2</sub> nanorods. ....	76
<b>Figure 3.8:</b> X-Ray photoelectron spectra of Mn 2p for (a) $\alpha$ -MnO <sub>2</sub> , (b) $\beta$ - MnO <sub>2</sub> and (c) $\alpha\beta$ - MnO <sub>2</sub> nanorods.....	78
<b>Figure 3.9:</b> X-Ray photoelectron spectra of O 1s for (a) $\alpha$ -MnO <sub>2</sub> , (b) $\beta$ - MnO <sub>2</sub> and (c) $\alpha\beta$ -MnO <sub>2</sub> nanorods. ....	79

<b>Figure 3.10:</b> Cyclic voltammogram of as prepared $\alpha$ -MnO <sub>2</sub> , $\beta$ - MnO <sub>2</sub> and $\alpha\beta$ - MnO <sub>2</sub> nanorods at the scan rate of 20 mV/sec. ....	81
<b>Figure 3.11:</b> Temperature dependent magnetization (M-T) curve of (a) $\alpha$ -MnO <sub>2</sub> , (b) $\beta$ -MnO <sub>2</sub> and (c) $\alpha\beta$ - MnO <sub>2</sub> nanorods. ....	84
<b>Figure 3.12:</b> Inverse susceptibility versus temperature fitted with Curie-Weiss law for (a) $\alpha$ -MnO <sub>2</sub> , (b) $\beta$ - MnO <sub>2</sub> and (c) $\alpha\beta$ - MnO <sub>2</sub> nanorods. ....	85
<b>Figure 3.13:</b> Magnetization versus magnetic field at 2K for (a) $\alpha$ -MnO <sub>2</sub> , (b) $\beta$ - MnO <sub>2</sub> and (c) $\alpha\beta$ - MnO <sub>2</sub> nanorods. Inset shows the enlarged view.....	86
<b>Figure 3.14:</b> Temperature dependence of real ( $\chi'$ ) and imaginary ( $\chi''$ ) of ac susceptibility data at 31, 101, 299 and 501 Hz with an ac field of 3 Oe for (a) $\alpha$ -MnO <sub>2</sub> , (b) $\beta$ - MnO <sub>2</sub> and (c) $\alpha\beta$ - MnO <sub>2</sub> nanorods and corresponding inset shows the enlarge view at peak position. 89	
<b>Figure 3.15:</b> Variation of relaxation time ( $\tau$ ) with temperature (T) plotted and fitted with (a) Neel-Arrhenius law (b) Vogel–Fulcher law and (c) Power law for $\alpha\beta$ - MnO <sub>2</sub> nanorods. Solid line represents the fitting. ....	92
<b>Figure 3.16:</b> Thermoremanent magnetization measurement at 5 K fitted with stretched exponential decay functions for (a) $\beta$ -MnO <sub>2</sub> and (b) $\alpha\beta$ -MnO <sub>2</sub> nanorods. ....	94
<b>Figure 4.1:</b> X-ray diffraction pattern of $\delta$ -MnO <sub>2</sub> . ....	99
<b>Figure 4.2:</b> FTIR spectrum of $\delta$ -MnO <sub>2</sub> . ....	100
<b>Figure 4.3:</b> Raman spectroscopy of $\delta$ -MnO <sub>2</sub> . ....	101
<b>Figure 4.4:</b> (a) Low resolution and (b) high resolution image of Transmission electron micrograph of $\delta$ -MnO <sub>2</sub> . Inset shows the particle size distribution histogram, (c) High resolution TEM and (d) SAED pattern of $\delta$ -MnO <sub>2</sub> .....	102
<b>Figure 4.5:</b> X-ray photoelectron spectroscopy of (a) Mn 2p and (b) O 1s of $\delta$ -MnO <sub>2</sub> . ....	103
<b>Figure 4.6:</b> (a) Temperature dependent magnetization (M-T) curve of $\delta$ -MnO <sub>2</sub> measured under applied field of 100 Oe. (b) shows the derivative dM/dT with temperature and (c) shows the inverse susceptibility versus temperature fitted with Curie-Weiss law in paramagnetic region.....	106
<b>Figure 4.7:</b> Temperature dependent magnetization (M-T) curve of $\delta$ -MnO <sub>2</sub> measured under applied field of (a) 50, 100, 500 Oe, and (b) 10 kOe. (c) shows the field dependence of reduced temperature with the best fit in terms of A-T line.....	108
<b>Figure 4.8:</b> (a) Magnetization vs. magnetic field at (a) 2, 10 and 30 K under ZFC and at (b) 2K under FC of $\delta$ -MnO <sub>2</sub> . ....	110

<b>Figure 4.9:</b> Temperature dependence of real, $\chi'$ and imaginary, $\chi''$ of ac susceptibility at 31, 101, 299 and 501 with ac field of 3 Oe. The inset shows the enlarged view of the peak shift with frequency. ....	112
<b>Figure 4.10:</b> (a) Variation of relaxation time $\tau$ with temperature $T_b$ plotted as $\ln\tau$ versus $(T_b)^{-1}$ and fitted with Neel-Arrhenius law, (b) Vogel-Fulcher law and power law (inset). 114	114
<b>Figure 4.11:</b> Thermoremanent magnetization measurement at 5K fitted with (a) Power law, Logarithmic decay (inset) and (b) Stretched exponential decay functions. ....	116
<b>Figure 5.1:</b> XRD of bare $\alpha$ -MnO <sub>2</sub> and $\alpha$ -MnO <sub>2</sub> : Dy (5, 10, 15, 20 mol %) nanorods. ....	121
<b>Figure 5.2:</b> Raman spectra of bare $\alpha$ -MnO <sub>2</sub> and $\alpha$ -MnO <sub>2</sub> : Dy (5, 10, 15, 20 mol %) nanorods. Inset shows the enlarge view of Raman band at 633 cm <sup>-1</sup> . ....	123
<b>Figure 5.3:</b> FE-SEM images of (a) bare $\alpha$ -MnO <sub>2</sub> , (b) $\alpha$ -MnO <sub>2</sub> : Dy (15 mol %) (c) $\alpha$ -MnO <sub>2</sub> : Dy (20 mol %) nanorods. ....	124
<b>Figure 5.4:</b> Particle size distribution histograms of bare $\alpha$ -MnO <sub>2</sub> and $\alpha$ -MnO <sub>2</sub> : Dy (15 and 20 mol %) nanorods. ....	125
<b>Figure 5.5:</b> TEM and HR-TEM images (a,b) for bare and (c, d) for $\alpha$ -MnO <sub>2</sub> : Dy (15 mol %) nanorods. SEAD patterns are shown in the inset of (b) and (d). ....	126
<b>Figure 5.6:</b> (a) Nitrogen adsorption desorption isotherms of bare and $\alpha$ -MnO <sub>2</sub> : Dy (5, 10 and 15 mol %) nanorods and (b) shows the corresponding pore size distribution. ....	128
<b>Figure 5.7:</b> Electrochemical performances of bare and $\alpha$ -MnO <sub>2</sub> : Dy (5, 10, 15, 20 mol %) nanorods (a) at 5 mV/sec (b) Specific capacitance Vs. Dy concentration (c) $\alpha$ -MnO <sub>2</sub> : Dy (15 mol %) at various scan rate and (d) specific capacitance at different scan rate. ....	131
<b>Figure 5.8:</b> Relationship between the maximum current and square root of the scan rate of bare and $\alpha$ -MnO <sub>2</sub> : Dy (5, 10, 15, 20 mol %) nanorods. ....	132
<b>Figure 5.9:</b> (a) Galvanostatic charge discharge at 10 A/g, (b) specific capacitance at various current density of bare and $\alpha$ -MnO <sub>2</sub> : Dy (5,10,15,20 mol%) nanorods, (c) charge discharge at different current densities and (d) cycling performance at the current density of 2 A/g of $\alpha$ -MnO <sub>2</sub> : Dy (15 mol %). ....	134
<b>Figure 5.10:</b> (a) Nyquist plot showing charge transfer resistances and inset shows the electrical equivalent circuit for bare and $\alpha$ -MnO <sub>2</sub> : Dy (5,10,15 & 20 mol%) nanorods and (b) Bode images of bare and $\alpha$ -MnO <sub>2</sub> : Dy (5,10,15,20 mol%) nanorods. ....	137
<b>Figure 6.1:</b> (1) X-ray photoelectron spectroscopy for Mn 2p in (a) $\alpha$ -MnO <sub>2</sub> (b) $\alpha$ -MnO <sub>2</sub> :Dy, (2) Dy 4d in $\alpha$ -MnO <sub>2</sub> and (3) for O1s in (a) $\alpha$ -MnO <sub>2</sub> and (b) $\alpha$ -MnO <sub>2</sub> :Dy nanorods. ....	141

<b>Figure 6.2:</b> Temperature dependent magnetization of (a) $\alpha$ -MnO <sub>2</sub> and $\alpha$ -MnO <sub>2</sub> :Dy under ZFC and FC. ....	144
<b>Figure 6.3:</b> The inverse susceptibility, $1/\chi$ Vs. T data in paramagnetic region is fitted with the equation $\chi^{-1} = T/C + 1/\chi_0 - b/(T-\theta)$ for (a) $\alpha$ -MnO <sub>2</sub> and (b) $\alpha$ -MnO <sub>2</sub> :Dy measured at an external applied field of 100 Oe. ....	144
<b>Figure 6.4:</b> Field dependent magnetization M(H) for ZFC at 2K, 15K and 30K of $\alpha$ -MnO <sub>2</sub> and $\alpha$ -MnO <sub>2</sub> :Dy nanorods.....	147
<b>Figure 6.5:</b> (a) Field dependent magnetization M(H) for FC under the field of 10 kOe at 2K of $\alpha$ -MnO <sub>2</sub> and $\alpha$ -MnO <sub>2</sub> :Dy nanorods. Upper inset shows the corresponding coercivity at positive field of $\alpha$ -MnO <sub>2</sub> . (b) Shows the variation of exchange bias with cooling field for both samples. ....	148
<b>Figure 6.6:</b> Schematic of core shell model of $\alpha$ -MnO <sub>2</sub> and $\alpha$ -MnO <sub>2</sub> :Dy nanorods having diameter 40 and 20 nm, respectively. The arrows indicate the magnetic state of the spins after initial magnetization. ....	150
<b>Figure 6.7:</b> Variation of thermoremanent remnant magnetization [M(t)] at 2K for $\alpha$ -MnO <sub>2</sub> and $\alpha$ -MnO <sub>2</sub> :Dy (in inset) nanorods. ....	151
<b>Figure 6.8:</b> (a) Enlarge view of five hysteresis loops to reveal the shift of the loop with increasing loop number for $\alpha$ -MnO <sub>2</sub> , (b) Variation of coercive fields Hc <sub>1</sub> and Hc <sub>2</sub> with number of recurrent hysteresis loops n. ....	154
<b>Figure 6.9:</b> symbols represent the experimental data for H <sub>EB</sub> versus loop index number (n). Dotted line corresponds to a fit with a power law for $n \geq 2$ , while solid line illustrates the best fit with equation 6.9.....	155



## *List of Tables*

<b>Table 1.1:</b> Crystallographic data of polymorphs of MnO <sub>2</sub> . .....	4
<b>Table 1.2:</b> Polymorphs of MnO <sub>2</sub> with different morphologies and their specific capacitance.....	32
<b>Table1.3:</b> Comparison of specific capacitance of cation-doped-MnO <sub>2</sub> nanostructures reported in literatures.....	35
<b>Table1.4:</b> Comparison of the specific capacitance of MnO <sub>2</sub> nanocomposites reported in the literature.....	36
<b>Table 3.1:</b> Structural parameters obtained from Rietveld refinement fitting for (a) $\alpha$ -MnO <sub>2</sub> , (b) $\beta$ -MnO <sub>2</sub> and (c) $\alpha\beta$ - MnO <sub>2</sub> nanorods. ....	72
<b>Table 3.2:</b> Mn <sup>+3</sup> /Mn <sup>+4</sup> and O <sub>b</sub> /O <sub>a</sub> obtained from fitting of Mn 2p and O 1s XPS peaks using software XPS peak 4.1 for $\alpha$ -MnO <sub>2</sub> , $\beta$ - MnO <sub>2</sub> and $\alpha\beta$ - MnO <sub>2</sub> nanorods.....	80
<b>Table 3.3:</b> Fitting parameters deduced from ac susceptibility data fitted with Neel-Arrhenius law, Power law and Vogel-Fulcher law for $\alpha\beta$ - MnO <sub>2</sub> nanorods.....	91
<b>Table 3.4:</b> Fitting parameters deduced from thermoremanent relaxation magnetization fitted with stretched exponential decay function for (1) $\beta$ - MnO <sub>2</sub> and (2) $\alpha\beta$ - MnO <sub>2</sub> nanorods.....	93
<b>Table 4.1:</b> Fitting parameters deduced from thermo remanant relaxation magnetization fitted with empirical relations like power law decay, logarithmic decay and stretched exponential decay functions.....	117
<b>Table 5.1:</b> Data obtained from EDAX for Dy in $\alpha$ -MnO <sub>2</sub> : Dy (5, 10, 15 and 20 mol %).	125
<b>Table 5.2:</b> Parameters obtained from Nitrogen adsorption desorption isotherm of bare and $\alpha$ -MnO <sub>2</sub> : Dy (5, 10 and 15 mol %) nanorods.....	129
<b>Table 5.3:</b> Comparison of specific capacitance of metal oxides reported in literatures with the present material, $\alpha$ -MnO <sub>2</sub> : Dy (15 mol %). ....	133
<b>Table 5.4:</b> EIS fitted parameters of bare MnO <sub>2</sub> and $\alpha$ -MnO <sub>2</sub> : Dy (5, 10, 15 and 20 mol %). .....	138
<b>Table 6.1:</b> Numeric value of exchange bias field and percentage of training effect during each cycle for bare and Dy doped $\alpha$ -MnO <sub>2</sub> . ....	152
<b>Table 6.2:</b> Values of the expression 6.9 fitting parameters approximating experimental data for training effect. ....	156



## *Abbreviations*

TMOs	Transition metal oxides
MnO <sub>2</sub>	Manganese Dioxide
NPs	Nanoparticles
OMSs	Octahedral molecular sieves
1D	One dimensional
2D	Two dimensional
3D	Three dimensional
FM	Ferromagnetic
T <sub>C</sub>	Curie temperature
M <sub>R</sub>	Remanant magnetization
H <sub>C</sub>	Coercive field
AFM	Antiferromagnetism
T <sub>N</sub>	Neel temperature
SG	Spin-glass
T <sub>f</sub>	Freezing temperature
ZFC	Zero field cooling
FC	Field cooling
DE	Double exchange
EDLC	Electrical double layer capacitor
CV	Cyclic voltammogram
PVP	Polyvinyl pyrrolidone

CTAB	Cetyltrimethylammonium bromide
NaOH	Sodium hydroxide
MWI	Microwave Irradiation
H <sub>EB</sub>	Exchange bias
RE	Rare earth
CNTs	Carbon nanotubes
CNFs	Carbon nanofibers
MCNT	Multiwall carbon nanotube
PCNF	Porus Carbon nanofibers
GCD	Galvanostatic charge discharge
EIS	Electrochemical impedance spectroscopy
XRD	X-ray diffraction
FTIR	Fourier Transform Infrared Spectroscopy
SEM	Scanning electron microscope
EDX	Energy Dispersive X-ray Spectroscopy
TEM	Transmission Electron Microscope
HRTEM	High Resolution Transmission Microscope
XPS	X-ray Photoelectron Spectroscopy
KE	Kinetic Energy
BE	Binding Energy
BET	Brunauer, Emmett, and Teller
BJH	Barrett-Joyner-Halenda
VSM	Vibrating Sample Magnetometer
SQUID	Superconducting Quantum Interface Device
SC	Specific capacitance

WE	Working electrode
RE	Reference electrode
CE	Counter electrode
GCE	Glassy Carbon Electrode
$\Theta_{CW}$	Curie Weiss Temperature
MT	Temperature dependent magnetization
MH	Field dependent magnetization
$T_{irr}$	Irreversible temperature
$\mu_{eff}$	Effective magnetic moment
CG	Cluster-glass
SPM	Superparamagnetic
AT	Almeida-Thouless
$T_{SG}$	Spin-glass transition temperature
$C_p$	Pseudocapacitance
$C_{dl}$	Double layer capacitance
$R_s$	Solution resistance
$R_{ct}$	Charge transfer resistance



## ***PREFACE***

Nanostructured transition metal oxides (TMOs) is probably one of the most interesting class of solids, exhibiting a wide range of crystal structures, great chemical stability and low-cost production. They are the compounds in which transition metal bound with oxygen atom forms a metal-oxygen bond whose nature varies from ionic to covalent or metallic. TMOs have an unusual number of accessible stable oxidation states per element with partially filled outer-d orbitals lead to characteristic properties such as magnetism due to the presence of unpaired electrons, which attract the interest of researchers. Among other inorganic TMOs, Manganese dioxide is an important functional metal oxide with half-filled outer d-orbital exhibits +4 oxidation state of Mn. Nanostructured MnO<sub>2</sub> has rich structural flexibility which adopts various crystallographic forms depending upon the size of the tunnel owing to their distinctive physical and chemical properties, as well as their wide applications in catalysts, component of the dry cell (Leclanché cell), inorganic pigment in ceramics, electrodes for electrochemical batteries (lithium, magnesium, sodium), and electrodes for supercapacitors. Such a great interest in MnO<sub>2</sub> is also due to its low price, toxicity, environmental friendliness and relative abundance in nature. The sharing of edges and vertices of basic MnO<sub>6</sub> octahedral unit with different linkage gives rise to  $\alpha$ ,  $\beta$ ,  $\delta$  and  $\gamma$  phase of MnO<sub>2</sub>. In  $\alpha$ -MnO<sub>2</sub>, the size of (2 × 2) tunnel is ~4.6 Å, which is required to stabilize through insertion/extraction of alkali cations such as Li<sup>+</sup>, Na<sup>+</sup>, K<sup>+</sup>, NH<sup>4+</sup>, Ba<sup>2+</sup>, or H<sub>3</sub>O<sup>+</sup>. 1D (1x1) tunnel structure pyrolusite,  $\beta$ -MnO<sub>2</sub> of size 1.89 Å is composed of a single strand of edge-sharing MnO<sub>6</sub> octahedra which can't accommodate cations because of its narrow size. 2D layers of edge shared MnO<sub>6</sub> octahedra form birnessite,  $\delta$ -MnO<sub>2</sub> with an interlayer separation of ~7 Å. The sheets of MnO<sub>6</sub> octahedra can be stabilized by inserting

a significant amount of water molecules or cations such as  $\text{Na}^+$  or  $\text{K}^+$  between them. The morphology, porosity and surface area strongly affect the physical and chemical properties of  $\text{MnO}_2$ . Several authors have demonstrated the constructive modifications in the structure and morphology, making it a practical tool for studying their effects on magnetic and electrochemical properties as well. As a result, the synthesis and study of the properties of  $\text{MnO}_2$  in different morphologies and structures for a wide range of applications are crucial. Rich varieties in magnetic properties of  $\text{MnO}_2$  come from differences in composition and structure which are provoked by distinct synthesis pathways and the presence of a large number of cations within the tunnels. Depending on the synthesis technique, sputtered grown  $\alpha$ - $\text{MnO}_2$  nanorods possess an exchange bias of 1340 Oe for 30 kOe field cooled M-H plot [1] whereas  $\alpha$ - $\text{MnO}_2$  nanoribbons synthesized through molten salt method possess a large zero-field cooling exchange bias of 1100 Oe [2]. *Luo et al.* have obtained that  $\alpha$ - $\text{K}_x\text{MnO}_2$  ( $x \leq 0.07$ ) show antiferromagnetic ordering below 24.5K, while  $\alpha$ - $\text{K}_{0.166}\text{MnO}_2$  single crystals show an antiferromagnetic ordering below 18 K [3][4]. The magnetic properties of  $\alpha$ - $\text{MnO}_2$  nanotubes have been tuned by intercalating Na, Li, and K cations within the tunnels. The doping concentration of  $\text{K}^+$  affects the magnetic ordering in  $\alpha$ - $\text{MnO}_2$  nanotubes. When the concentration of  $\text{K}^+$  is  $\leq 12$  at%, it shows ferromagnetic behaviour and with doping concentration more than 12 at %, it shows antiferromagnetic behaviour [5]. The structure and magnetic properties of hydrothermally synthesized  $\beta$ - and  $\alpha$ - $\text{K}_x\text{MnO}_2$  ( $x = 0.15$  and  $0.18$ ) nanorods are thoroughly investigated by *Barudzija et al.*  $\beta$ - $\text{MnO}_2$  exhibits AFM transition at 93 K, while both  $\alpha$ - $\text{K}_x\text{MnO}_2$  ( $x = 0.15$  and  $0.18$ ) nanorods possess reentrant spin-glass type behaviour at  $T_f = 21$  K and 20 K, respectively [6].

On the other hand, morphology, porosity and surface area also affect the electrochemical properties of MnO<sub>2</sub>. One can tune them by using different synthesis techniques and altering the synthesis parameters to improve pseudocapacitive performance. In this context, MnO<sub>2</sub> nanosphere, hollow urchin and smooth ball show quite high capacitance of 317, 204 and 276 Fg<sup>-1</sup> at a scan rate of 5 mV/s, respectively [7].  $\gamma$ -MnO<sub>2</sub> microspheres,  $\alpha$ - and  $\beta$ -MnO<sub>2</sub> nanorods possess specific capacitance of 237.6 Fg<sup>-1</sup>, 103.9 Fg<sup>-1</sup> and 57.7 Fg<sup>-1</sup> in 1M Na<sub>2</sub>SO<sub>4</sub> electrolyte at 5 mV/s, respectively [8]. In addition, dopants in  $\alpha$ -MnO<sub>2</sub> also may offer high specific capacitance as it possesses tunnel cavity of as large as 0.46 nm which is appropriate for the intercalation/de-intercalation of an external cation. *Tang et al.* achieve a significant improvement in specific capacitance (415 F g<sup>-1</sup> at 0.2 A g<sup>-1</sup>) for Co doped MnO<sub>2</sub> spheres, double than that of MnO<sub>2</sub> spheres (231 F g<sup>-1</sup>) [9]. MnO<sub>2</sub> nanoflowers with specific capacitance of 160 Fg<sup>-1</sup> transforms into MnO<sub>2</sub> orchids having high capacitance 202 Fg<sup>-1</sup> after doping Cr [10]. Many efforts have been made by various researchers to increase the specific capacitance by synthesizing various doped MnO<sub>2</sub> nanostructured materials under different physical conditions.

### **Important findings of the present work**

Our thorough investigations focus detailed study on the influence of the synthesis parameters on polymorphic structures and properties of MnO<sub>2</sub> nanostructures. These are the important factors for tailoring the features required for certain applications. The structural, magnetic and electrochemical properties of polymorphs of MnO<sub>2</sub> and the effect of Dy doping in MnO<sub>2</sub> have revealed several key findings which we have reported and published in peer reviewed journals. Some of the important results are listed below:

1. Detailed investigations on magnetic properties of  $\alpha$ ,  $\beta$ , and mixed phase of  $\alpha$  and  $\beta$ - $\text{MnO}_2$  by understanding their magnetic transitions and spin-glass behaviour based on different concentration of  $\text{Mn}^{3+}/\text{Mn}^{4+}$  in each sample has been discussed using XRD, Raman, XPS, magnetization, ac susceptibility and remanant magnetization measurement.  $\alpha$ ,  $\beta$ , and mixed phase of  $\alpha$  and  $\beta$ - $\text{MnO}_2$  have been successfully synthesised through hydrothermal technique by varying the concentration of potassium ion. XRD and FTIR spectroscopy confirmed the pure phase formation of  $\text{MnO}_2$ . Rietveld refinement reveals the phase fraction of  $\alpha$  and  $\beta$  phase to be  $\sim 73\%$  and  $\sim 27\%$ , respectively in  $\alpha\beta$ - $\text{MnO}_2$ . SEM micrograph shows that the polymorphic phases crystalize in the form of nanorods. Small size of nanorods in  $\beta$ - $\text{MnO}_2$  resulted high specific capacitance in comparison to  $\alpha$ - and  $\alpha\beta$ - $\text{MnO}_2$  nanorods. XPS confirms the presence of large concentration of  $\text{Mn}^{3+}$  in  $\alpha$ - and  $\alpha\beta$ - $\text{MnO}_2$  nanorods results high effective magnetic moment and high optical band gap. Negative Curie-Weiss temperature ( $\theta_{\text{cw}}$ ) while confirmed the antiferromagnetic ordering in  $\alpha$ - $\text{MnO}_2$  and  $\alpha\beta$ - $\text{MnO}_2$ , positive  $\theta_{\text{cw}}$  in  $\beta$ - $\text{MnO}_2$  showed strong ferromagnetic interaction due to dominating intra sublattice interaction. No shifting of the peak in  $\chi'$  (T) in ac susceptibility ruled out the presence of spin-glass behaviour in  $\alpha$ - $\text{MnO}_2$  nanorods. However, in  $\beta$ - $\text{MnO}_2$  and  $\alpha\beta$ - $\text{MnO}_2$ ,  $T_f$  observed at 22 K and 19 K absent in M Vs. T curve showed frequency dispersion behaviour. SG behaviour was critical towards the presence of  $\text{Mn}^{3+}$  in  $\text{MnO}_2$  compound which also affects the bandgap of the material.
2. Monoclinic,  $P6_3/mnm$  structure of  $\delta$ - $\text{MnO}_2$  has been synthesised through a facile hydrothermal technique. XRD, FT-IR and Raman spectroscopy confirmed the formation of the  $\delta$  phase of  $\text{MnO}_2$ . Temperature-dependent susceptibility confirms the

strong antiferromagnetic ordering and high effective magnetic moment attributed to the presence of both  $\text{Mn}^{3+}$  and  $\text{Mn}^{4+}$ , as confirmed by XPS. The reduced valency of Mn from 4 to 3 is accompanied with oxygen vacancies, affording the exact composition of  $\text{MnO}_{1.58}$ . DC magnetization showed the existence of an AT-type phase boundary with the freezing of spin clusters at 11.2 K. The dynamic magnetic properties of the  $\delta\text{-MnO}_2$  were investigated using the frequency-dependent ac susceptibility fitted with various phenomenological models like the Vogel–Fulcher law and power law, indicating the existence of interacting spin clusters, which could freeze at 11.2 K. The time dependence of thermoremanent magnetization fitted well with a stretched exponential function, supporting the existence of relaxing spin clusters. Thus, the spin glass relaxation in the  $\delta\text{-MnO}_2$  is attributed to the interaction between  $\text{Mn}^{4+}$  and  $\text{Mn}^{3+}$ , which results in intrinsic magnetic frustration.

3. Tetragonal,  $I4/m$  structure of  $\alpha\text{-MnO}_2$  nanorods with different concentration of Dy were synthesised via simple one step hydrothermal method. Incorporation of Dy ion not only influenced the crystalline nature but also inhibited the growth of nanorods. With increasing Dy concentration in  $\alpha\text{-MnO}_2$  although, the structure of  $\text{MnO}_2$  remained tetragonal, the crystallinity deteriorated and inhibited the growth rate of nanorods. We observe that when the concentration of Dy reached to 15 mol%, the diameter and length of  $\alpha\text{-MnO}_2$  nanorods reduced from 40 nm and 4-5  $\mu\text{m}$  to 20 nm and 70 nm, respectively. Being  $\text{MnO}_2$  as a good electroactive material, a significant enhancement in specific capacitance accompanied with a decrease in charge transfer resistance after incorporating 15 mol% Dy was observed. Such enhancement in specific capacitance attributed to poor crystallinity along with large surface area and pore size distribution.

Here we concluded that rare earth doped  $\alpha$ -MnO<sub>2</sub> can be explored as an eminent electrode material for an application of supercapacitor.

4.  $\alpha$ -MnO<sub>2</sub> and  $\alpha$ -MnO<sub>2</sub>:Dy (15 mol%) nanorods of diameter 40 and 20 nm are further characterized to study the effect of Dy doping on their magnetic properties. Neel temperature of  $\alpha$ -MnO<sub>2</sub> was found to be 18 K less than that of bulk  $\alpha$ -MnO<sub>2</sub> ( $T_N = 24.5$  K) and further decreased to 11 K after doping Dy with an increasing antiferromagnetic interaction. The existence of exchange bias was found in both samples by observing a clear shift in field cooled M-H loops. For  $\alpha$ -MnO<sub>2</sub>, large  $H_{EB}$  of 565 Oe was obtained which decreased to 140 Oe after doping Dy at the cooling field of 30 kOe. Such variation of exchange bias field was understood on the basis of core shell structure which consists of frozen and rotatable spins in the core and surface of nanorods respectively. The competition between core and surface spins depending on the size of nanorods thus decides the spin-glass behaviour, EB field observed in these nanorods. Change in exchange bias field with consecutive cycles showing the training effect has been discussed after fitted with phenomenological models like Power law and multiple exponent function.

**This thesis is organized into VII chapters:**

**Chapter I** A brief introduction and literature survey on MnO<sub>2</sub> is presented.

**Chapter II** describes the synthesis technique for the preparation of the polymorphs of MnO<sub>2</sub> ( $\alpha$ ,  $\beta$  and  $\delta$ -MnO<sub>2</sub>) and Dy doped  $\alpha$ -MnO<sub>2</sub>. It also includes the synthesis method used for the preparation of electrode for electrochemical characterization. Working electrode was prepared by drop casting synthesised active material on tore paper of area 1 cm<sup>2</sup>. A concise overview of the instruments is provided which are used for structural

characterization of MnO<sub>2</sub> through XRD, for particle morphology SEM and UV visible spectroscopy for optical bandgap. XPS is used for elemental analysis and magnetic properties are studied using MPMS. An electrochemical workstation (CHI 7044) was used to study the electrochemical performances of the samples by performing cyclic voltammetry (CV), Galvanostatic charge discharge (GCD) and electrochemical impedance spectroscopy (EIS) using electrochemical three electrode cell in 1M Na<sub>2</sub>SO<sub>4</sub> electrolyte solution.

**Chapter III** deals with the structural, magnetic and electrochemical properties of  $\alpha$ -,  $\beta$ - and mixed phase of  $\alpha$  and  $\beta$  MnO<sub>2</sub> nanorods.

**Chapter IV** includes the study of structure and magnetic properties of  $\delta$ -MnO<sub>2</sub>.

**Chapter V** shows the influence of Dy doping on electrochemical properties of  $\alpha$ -MnO<sub>2</sub> nanorods. For  $\alpha$ -MnO<sub>2</sub>: Dy (15 mol %), capacitance enhances by twice than that of bare  $\alpha$ -MnO<sub>2</sub>.

**Chapter VII** The effect of Dy incorporation on magnetic properties of  $\alpha$ -MnO<sub>2</sub> nanorods. Change in exchange bias field with consecutive cycles showing the training effect has been discussed after fitting with phenomenological models.

**Chapter VII** summarizes the main findings of the present work. We present the future works to be done in this area.

*List of publications, journals and books used to bind up the thesis has been given at the end of the thesis as references.*